Electrical circuit modeling of reversed field pinches

J. C. Sprott
Department of Physics, University of Wisconsin, Madison, Wisconsin 53706

(Received 4 February 1988; accepted 4 May 1988)

Equations are proposed to describe the radial variation of the magnetic field and current density in a circular, cylindrical reversed field pinch (RFP). These equations are used to derive the electrical circuit parameters (inductance, resistance, and coupling coefficient) for a RFP discharge. The circuit parameters are used to evaluate the flux and energy consumption for various start-up modes and for steady-state operation using oscillating field current drive. The results are applied to the MST device [Bull. Am. Phys. Soc. 32, 1830 (1987)].

I. INTRODUCTION

A reversed field pinch (RFP)[1,2] can be modeled as a nonlinear, two-port electrical circuit element[3-5] in which the ports represent, respectively, the poloidal-field and the toroidal-field circuits as shown in Fig. 1. The existence of a close-fitting conducting shell near the plasma boundary conveniently divides the internal (plasma) region from the external region in which conventional electrical circuit analysis can be used. The shell typically has voltage gaps to allow the magnetic fields to enter. These gaps represent the ports across which the voltages V_p and V_t are prescribed. The currents into the ports are given, respectively, by the net plasma current I_p encircling the major axis and by the net current I_t in the toroidal-field windings.

Some of the current in the poloidal-field winding contributes to magnetizing the space through the hole in the toroid and is thus not reflected in current in the plasma. This magnetizing current, which is usually small in a device with an iron core, is considered part of the external circuit. If the shell has no gaps or if a resistive liner is inside but near the shell, the resulting current can be included in the external circuit.

We assume that the RFP has a circular cross section of minor radius a and that the major radius R_0 is large compared to a. In this cylindrical approximation, the subscript t is associated with the toroidal direction (parallel to the axis of the cylinder), p is associated with the poloidal (azimuthal) direction, and r is associated with the radial direction. The currents and fields are assumed to have poloidal and toroidal symmetry. The toroidal-field current and voltage are related to the internal fields by

$$I_t = 2\pi R_0 B_{tw}/\mu_0, \tag{1}$$

$$V_t = \pi a^2 \frac{d\langle B_t\rangle}{dt}, \tag{2}$$

where B_{tw} is the toroidal field at the wall ($r = a$) and $\langle B_t\rangle$ is the average toroidal field (toroidal flux divided by πa^2),

$$\langle B_t\rangle = \frac{2}{a^2}\int_0^a rB_t\, dr. \tag{3}$$

It is customary to define two dimensionless parameters, the field reversal parameter

$$F = B_{tw}/\langle B_t\rangle = \mu_0 I_t/2\pi R_0\langle B_t\rangle, \tag{4}$$

and the pinch parameter

$$\theta = B_{pw}/\langle B_t\rangle = \mu_0 I_p/2\pi a\langle B_t\rangle, \tag{5}$$

where B_{pw} is the poloidal field at the wall ($r = a$).

The goal of this paper is to provide simple formulas that can be used as part of a circuit simulation to predict the electrical performance of a RFP or to diagnose the plasma from the easily measured external voltages and currents. The electrical circuit parameters for the plasma are calculated under the assumption that the plasma relaxes to a preferred magnetic field profile and plasma current density profile in a time fast compared to the rate at which the external currents change. These profiles are calculated in Sec. II. From the profiles, the plasma inductance, resistance, and the coefficient of coupling between the ports are calculated in Sec. III. For those cases in which the calculations lead to a complicated expression, the result is displayed graphically and approximated to within a few percent by a simple analytic function. The circuit parameters are then used to determine the flux and energy requirements for both the poloidal-field and toroidal-field circuits for various start-up modes in Sec. IV.

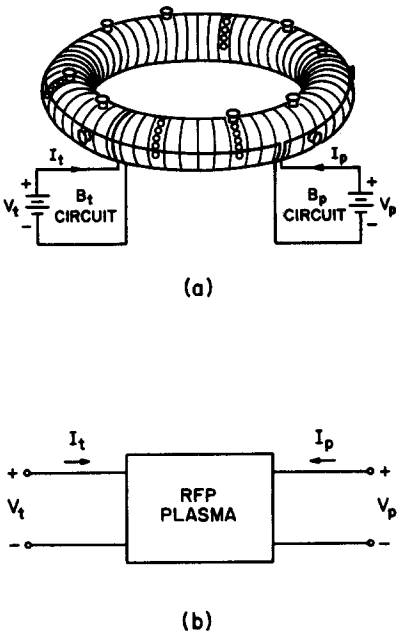

FIG. 1. A toroidal plasma such as a RFP (a) can be represented as a two-port electrical network (b) in which the toroidal-field and poloidal-field circuits represent the two ports. The current I_t is the net current in the toroidal-field windings, and the current I_p is the net current in the plasma encircling the major axis.

 0031-9171/88/082266-10$01.90

Also included in Sec. IV is a calculation of the oscillating voltages required to maintain a steady-state current in the presence of resistive losses. Finally, the results are applied to the University of Wisconsin MST device[6] in Sec. V.

II. RADIAL PROFILES

RFP plasmas are believed to relax on a relatively fast time scale to a unique spatial profile that depends only on the value of θ (or F) and which presumably represents a minimum energy state subject to some constraint. A number of such profile models have been discussed in the literature.[3,4,7–13] We consider here two models—the Bessel function model (BFM) which has the firmest theoretical base, and the polynomial function model (PFM) which is a modification of the BFM to agree better with experiment and to simplify calculations.

A. Bessel function model

In a classic paper,[7] Taylor showed that the minimum energy state of a pressureless plasma bounded by a perfectly conducting shell and subject to conservation of the total magnetic helicity has a plasma current density $\mathbf{j}$ parallel to and proportional to the magnetic field $\mathbf{B}$. Under the usual conditions ($\theta < 1.56$), the lowest energy state is axisymmetric, and in the cylindrical approximation the fields are given by

$$B_t = B_{t0} J_0(2\theta r/a), \quad B_p = B_{t0} J_1(2\theta r/a), \tag{6}$$

where B_{t0} is the toroidal field on axis ($r=0$) and θ is the pinch parameter given by Eq. (5). Here J_0 and J_1 are Bessel functions of zeroth and first order, respectively. The field reversal parameter is given in the Bessel function model by

$$F = \theta J_0(2\theta)/J_1(2\theta). \tag{7}$$

For what follows, it is useful to expand the Bessel function expressions for the fields, current density j and F as power series in θ, the first few terms of which are

$$\begin{aligned}
B_t/B_{t0} &= 1 - (\theta r/a)^2 \\
&\quad + (\theta r/a)^4/4 - (\theta r/a)^6/36 + \cdots, \\
B_p/B_{t0} &= \theta r/a - (\theta r/a)^3/2 \\
&\quad + (\theta r/a)^5/12 - \cdots, \\
\mu_0 a j_t/B_{t0} &= 2\theta - 2\theta(\theta r/a)^2 \\
&\quad + \theta(\theta r/a)^4/2 - \theta(\theta r/a)^6/18 + \cdots, \\
\mu_0 a j_p/B_{t0} &= 2\theta^2 r/a - \theta(\theta r/a)^3 \\
&\quad + \theta(\theta r/a)^5/6 - \cdots, \\
\langle B_t\rangle/B_{t0} &= 1 - \theta^2/2 + \theta^4/12 - \theta^6/144 + \cdots, \\
F &= 1 - \theta^2/2 - \theta^4/12 - \theta^6/48 - \theta^8/180 - \cdots.
\end{aligned} \tag{8}$$

The tokamak limit has $\theta \ll 1$ ($F \approx 1$), and the RFP state has $\theta > 1.202$ ($F < 0$). For $\theta > 1.202$, the field reversal surface is at a radius of $r_R = 1.202a/\theta$.

B. Polynomial function model

The difficulty with the BFM is that it assumes a pressureless plasma with a finite plasma current density at the wall in contrast to experiment in which the plasma pressure is typically 10%–20% of the magnetic pressure and the current density approaches zero at the wall.[1,14–16] The usual modified Bessel function model (MBFM) approach[3,4] is to assume $\mathbf{j}$ and $\mathbf{B}$ are parallel with j/B constant out to some radius (typically $0.7a$) beyond which it falls linearly to zero at $r=a$. We here propose a heuristic model whose primary virtue is its algebraic simplicity, although it is seen to agree with experiment as well as any of the other models. The strategy is to express the magnetic fields and current density as polynomial functions of radius subject to the following conditions:

$$\begin{aligned}
&\nabla\times\mathbf{B} = \mu_0 \mathbf{j}, \quad \mathbf{j} = 0 \quad \text{at} \quad r = a, \\
&\frac{d(\mathbf{j}\cdot\mathbf{B}/B^2)}{dr} = 0 \quad \text{at} \quad r = 0, \\
&\frac{d^2(\mathbf{j}\cdot\mathbf{B}/B^2)}{dr^2} = 0 \quad \text{at} \quad r = 0.
\end{aligned} \tag{9}$$

Enough terms in the polynomials are kept to satisfy these conditions exactly, leading to unique profiles for $\mathbf{j}$ and $\mathbf{B}$,

$$\begin{aligned}
B_t/B_{t0} &= 1 - \theta_0^2 (r/a)^2 + \theta_0^2 (r/a)^4/2, \\
B_p/B_{t0} &= \theta_0 r/a - \theta_0^3 (r/a)^3/2 \\
&\quad + \theta_0(\theta_0^2 - 1)(r/a)^5/3, \\
\mu_0 a j_t/B_{t0} &= 2\theta_0 - 2\theta_0^3 (r/a)^2 \\
&\quad + 2\theta_0(\theta_0^2 - 1)(r/a)^4, \\
\mu_0 a j_p/B_{t0} &= 2\theta_0^2 r/a - 2\theta_0^2 (r/a)^3,
\end{aligned} \tag{10}$$

where θ_0 ($= \mu_0 a j_{t0}/2B_{t0}$) is the value that θ would have if $\mathbf{j}\cdot\mathbf{B}/B^2$ were a constant with the same value that it has at $r=0$. In terms of F, θ_0 is given by

$$\theta_0 = [(6 - 6F)/(3 - 2F)]^{1/2}. \tag{11}$$

The pinch parameter is

$$\theta = \theta_0(4 - \theta_0^2)/(6 - 2\theta_0^2), \tag{12}$$

and the average toroidal field is

$$\langle B_t\rangle/B_{t0} = 1 - \theta_0^2/3. \tag{13}$$

It is interesting to note the similarity of Eqs. (10) and (13) to Eq. (8). Note also that $F=0$ occurs when θ and θ_0 are 1.414 in the PFM in contrast to the value of 1.202 in the BFM.

The PFM radial profiles of $\mathbf{B}$ and $\mathbf{j}$ are shown in Fig. 2 for a typical RFP value of $\theta = 1.5$ corresponding to $F = -0.1232$, along with the BFM at $\theta = 1.441$ (giving the same θ_0 for each). The differences are not extreme, but become more so as $|F|$ increases.

In contrast to the BFM, $\mathbf{j}$ is not precisely parallel to $\mathbf{B}$ in the PFM. This fact is illustrated in Fig. 3(a) in which the quantities

$$\begin{aligned}
\lambda_{\parallel} &= \mathbf{j}\cdot\mathbf{B}/B^2 = (j_p B_p + j_t B_t)/(B_p^2 + B_t^2), \\
\lambda_{\perp} &= |\mathbf{j}\times\mathbf{B}|/B^2 = (j_t B_p - j_p B_t)/(B_p^2 + B_t^2)
\end{aligned} \tag{14}$$

normalized to $1/\mu_0 a$, are plotted versus radius. The existence of a small $\lambda_{\perp}$ is equivalent to assuming the plasma has finite pressure. From $\mathbf{j}\times\mathbf{B} = \nabla p$, the equivalent pressure calculated from

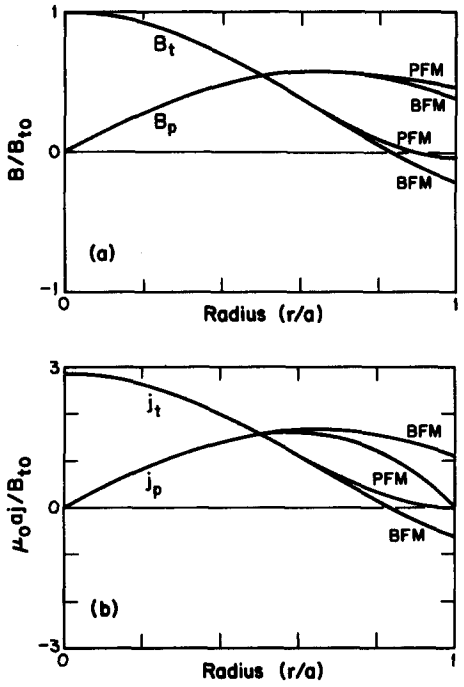

FIG. 2. Radial profiles of the toroidal and poloidal components of the magnetic field B and current density j for the polynomial function model (PFM) at $\theta = 1.5$. Also shown are the profiles for the Bessel function model (BFM) for the same value of j/B at $r = 0$.

$$p = \int_a^r (j_p B_t - j_t B_p) dr \tag{15}$$

and normalized to $B_{pw}^2/2\mu_0$ is plotted in Fig. 3(b) for several values of θ. Normalized in this way, the curves represent

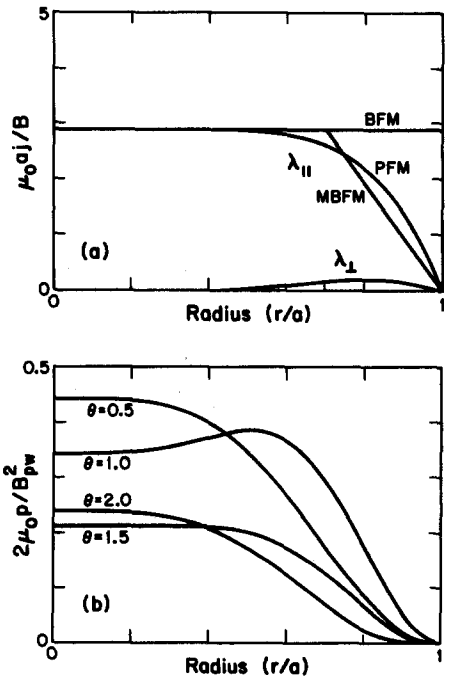

FIG. 3. Radial profiles of $\lambda_\parallel$ and $\lambda_\perp$ for the polynomial function model (PFM) at $\theta = 1.5$ (a) and the normalized plasma pressure implied by the nonzero $\lambda_\perp$ for various values of θ (b). The Bessel function model (BFM) by definition has $\lambda_\parallel$ constant and $\lambda_\perp = 0$ at all radii. The modified Bessel function model (MBFM) has $\lambda_\parallel$ constant for $r < 0.7a$ and $\lambda_\perp = 0$ everywhere.

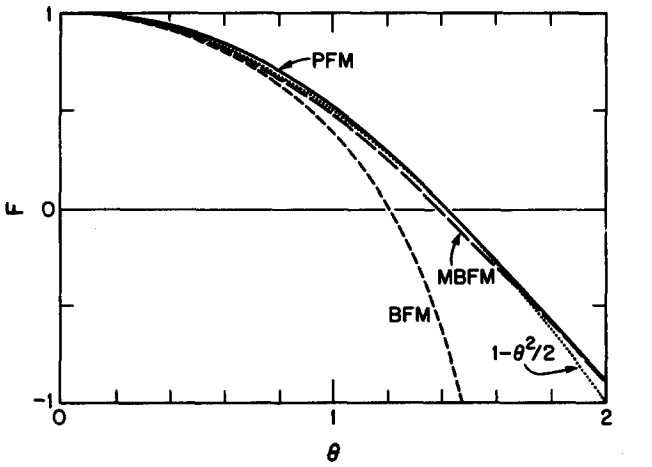

FIG. 4. F-θ curve for the polynomial function model (PFM), the Bessel function model (BFM), and the modified Bessel function model (MBFM) with a breakpoint at $r = 0.7a$. Also shown is a simple analytic function that closely fits the PFM and MBFM.

values of β_p. The $\theta = 1.5$ case has a pressure on axis about 21% of the poloidal-field magnetic pressure at $r = a$, and thus the PFM fortuitously mimics real, finite-pressure RFP devices.

A major point of comparison of the models with one another and with experiment is the F-θ curve as shown in Fig. 4. The PFM curve is given by

$$\theta = (3 - F)[(2 - 2F)/(9 - 6F)]^{1/2}, \tag{16}$$

and the BFM curve by Eq. (7). Also shown is the numerically evaluated MBFM result for a breakpoint at $r = 0.7a$. The PFM result can be fit to within 5% over the range of $0 < \theta < 1.7$ by the simple function

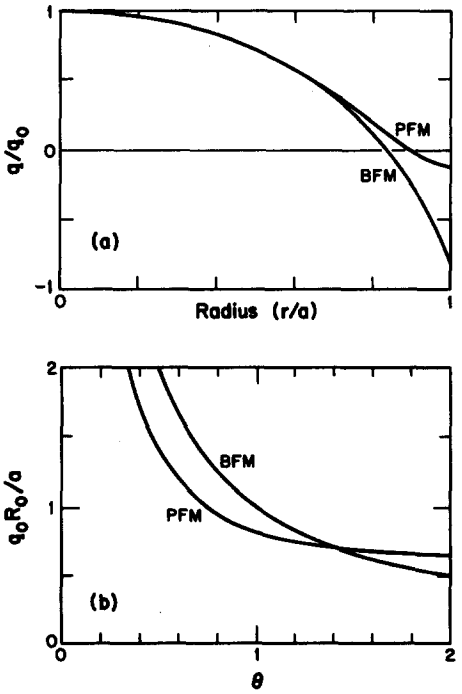

FIG. 5. Radial profile of safety factor q for the polynomial function model (PFM) at $\theta = 1.5$ and the Bessel function model (BFM) for the same value of j/B at $r = 0$, normalized to q_0, the value of q at $r = 0$ (a). The value of q_0 as predicted by the PFM is relatively independent of θ in the RFP state (b).

$$F \approx 1 - \theta^2/2, \tag{17}$$

which is just the first two terms of the BFM series in Eq. (8). With the PFM, reversal occurs at $\theta^2 = 2$ in good agreement with experiment.

The q profile given by

$$q = rB_t/R_0B_p \tag{18}$$

normalized to q_0 (the value of q on axis) is plotted in Fig. 5(a) for the BFM at $\theta = 1.441$ and the PFM at $\theta = 1.5$. A curious feature is the near constancy of q_0 for the PFM for $\theta \gtrsim 1.4$ as shown in Fig. 5(b). The value is

$$q_0 = [(3 - 2F)/(6 - 6F)]^{1/2} a/R_0, \tag{19}$$

or approximately $2a/3R_0$ in the RFP ($F<0$) state in good agreement with experiment.[12] The value of q_0 is asymptotic to $0.577a/R_0$ at large θ.

III. ELECTRICAL CIRCUIT PARAMETERS

Applying power balance to the electrical circuit of Fig. 1 gives

$$V_pI_p + V_tI_t = \frac{dU_m}{dt} + P_{\mathrm{Oh}}, \tag{20}$$

where U_m is the inductive energy stored in the magnetic field,

$$U_m = \frac{2\pi^2 R_0}{\mu_0} \int_0^a (B_p^2 + B_t^2) r\, dr, \tag{21}$$

which for the PFM evaluates to

$$U_m = \pi^2 R_0 a^2 B_{t0}^2 (1 - 17\theta_0^2/54 - \theta_0^4/270 + 31\theta_0^6/2160)/\mu_0, \tag{22}$$

and P_{Oh} is the Ohmic power dissipated by the plasma,

$$P_{\mathrm{Oh}} = 4\pi^2 R_0 \int_0^a \eta j_\parallel^2 r\, dr, \tag{23}$$

where η is the resistivity and $j_\parallel$ denotes the component of $\mathbf{j}$ parallel to $\mathbf{B}$. Included in P_{Oh} is the power that goes into increasing the stored thermal energy in the plasma as well as the energy lost from the plasma by radiation and other transport processes. To the extent that the plasma maintains a given F-θ relation, the magnetic energy can be written as a function of I_p and of $\langle B_t \rangle$ whose derivative is related to V_t by Eq. (2), and Eq. (20) can then be divided by I_p and rearranged to give

$$V_p = L\frac{dI_p}{dt} + AV_t + R_pI_p, \tag{24}$$

where L, A, and R_p are functions of θ (or F). Note that the quantity R_pI_p, which in the steady state is just the measured loop voltage, does not correspond to the integral of the electric field around any simple loop when the fields are changing. It is, nevertheless, a useful quantity for determining the net Ohmic input to the plasma and the conductivity temperature. In the following sections, these functions will be evaluated assuming PFM profiles.

A. Plasma inductance

Consider first a plasma confined in a flux-conserving shell ($V_t = 0$). The inductance can then be calculated from

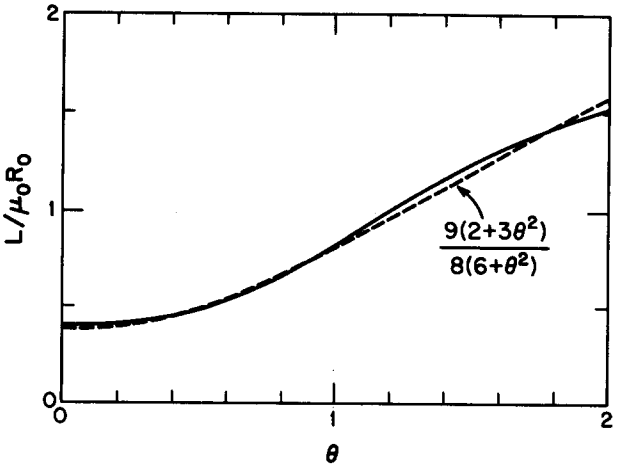

FIG. 6. Normalized plasma inductance with a flux-conserving shell as a function of θ along with a simple analytic fit.

$$L = \frac{1}{I_p}\frac{\partial U_m}{\partial I_p}\bigg|_{\langle B_t \rangle = \mathrm{const}}. \tag{25}$$

The analytic expression is cumbersome, but the result is displayed as a function of θ in Fig. 6 along with an empirical fit good to within 5% for $\theta < 2$,

$$L = 9\mu_0R_0(2 + 3\theta^2)/8(6 + \theta^2). \tag{26}$$

A fit of this type was chosen rather than a polynomial so that the inductance is well behaved at large θ as will be required for the calculation in Sec. IV D. The increase of inductance with θ is partly a result of the helical current path and partly a result of the peaking of the current density profile. Note that the inductance defined by Eq. (24) is only one of several inductances that one can define. It is useful for the calculation of the flux and energy requirements (Sec. IV) and for electrical circuit modeling (Sec. V).

B. Coupling coefficient

Now consider a plasma with I_p held constant by a high-impedance power supply in the poloidal-field circuit, but with a voltage V_t applied in such a way as to cause $\langle B_t \rangle$ to change in time. The result is to induce a voltage V_p proportional to V_t with a coefficient of proportionality given by

$$A = \frac{1}{\pi a^2 I_p}\frac{\partial U_m}{\partial \langle B_t \rangle}\bigg|_{I_p = \mathrm{const}} - \frac{R_0F}{a\theta}. \tag{27}$$

The first term represents $I_p\, dL/dt$ caused by modulation of the inductance by the varying $\langle B_t \rangle$, and the second term represents a direct transformerlike coupling of the two circuits through the helical field lines which behave like conducting wires. The terms are of the same order but of opposite sign. The result of evaluating Eq. (27) as a function of θ is shown in Fig. 7 along with an empirical fit,

$$A = 4R_0\theta(1 - \theta^2)/a(8 + 3\theta^3). \tag{28}$$

This coupling between the toroidal- and poloidal-field circuits is small for a tokamak ($\theta \ll 1$) but of considerable importance for a RFP ($\theta^2 > 2$).

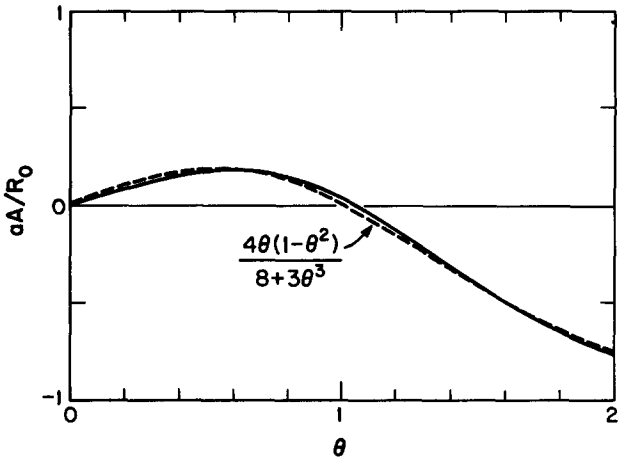

FIG. 7. Normalized coefficient of coupling between the poloidal-field and toroidal-field circuits as a function of θ along with a simple analytic fit.

C. Plasma resistance

Finally, consider a resistive plasma in steady state ($I_p = \text{const}$, $V_t = 0$) at a given value of θ. If the perpendicular conductivity is negligible and the parallel resistivity η is independent of radius, the resistance can be calculated from

$$R_p = \frac{4\pi^2 R_0 \eta}{I_p} \int_0^a \frac{(j_t B_t + j_p B_p)^2}{B_t^2 + B_p^2}\, r\, dr. \tag{29}$$

The result is displayed as a function of θ in Fig. 8 along with an empirical fit good to within 10% for all θ,

$$R_p \approx 22 R_0 \eta (5 + 6\theta^2)/5a^2(10 + \theta^2). \tag{30}$$

The rise of resistance with θ is caused partly by peaking of the current density profile, but more importantly by the increasing pitch of the field lines (the "screw-up factor"). This factor has been calculated for the BFM[17] and measured experimentally.[18] The normalized resistance for the PFM at $\theta = 0$ is 1.2, compared to 1.0 for a flat current density profile and $\frac{4}{3}$ for a parabolic profile.

The use of a spatially uniform resistivity is consistent with limited observations that RFP temperature profiles are relatively flat[19–21] but is not consistent with the observed current density profiles [Fig. 2(b)], which in the presence of a spatially uniform, toroidal electric field imply increasing resistivity (proportional to $1/j_t$) as $r \to a$. This discrepancy has been discussed elsewhere[4] and is evidence of a non-Ohmic contribution to the resistivity (the "dynamo").[22,23]

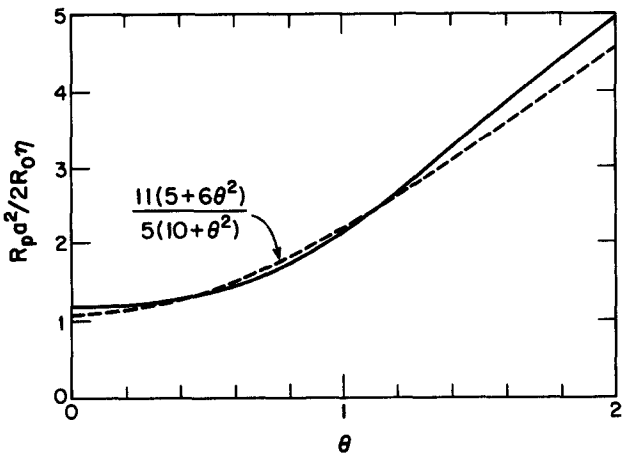

FIG. 8. Normalized plasma resistance as a function of θ along with a simple analytic fit.

One may define a "conductivity temperature" T_e (in eV) in such a way that the resistivity as defined above obeys the classical relation,[24]

$$\eta = 8 \times 10^{-4} Z_{\text{eff}} / T_e^{3/2}, \tag{31}$$

where the Coulomb logarithm has been taken as about 15 and Z_{eff} is the effective ionic charge. The conductivity temperature (with $Z_{\text{eff}} = 1.0$) can thus be determined from experimentally measured voltages and currents by the relation,

$$T_e = \left(\frac{8 \times 10^{-4} R_p I_p}{\eta (V_p - L\, dI_p/dt - A V_t)} \right)^{2/3}. \tag{32}$$

The temperature calculated in this way represents a reasonable lower bound on the actual electron temperature on the axis of a RFP.

IV. FLUX AND ENERGY REQUIREMENTS

The electrical circuit parameters of Sec. III can be used to calculate the flux and energy requirements for both the poloidal-field and toroidal-field sources in order to build the plasma current from an initial value of zero up to some final value I_{pf} with a final pinch parameter of θ_f. In this section, external inductance and resistance and resistive losses in the plasma will be neglected except as noted. The neglect of plasma resistance is equivalent to assuming that the plasma current reaches its maximum value in a time short compared to τ/β, where τ is the plasma energy confinement time and β is the ratio of plasma pressure to magnetic pressure. The neglect of resistance allows the problem to be cast in a time-independent form.

For the poloidal-field circuit, the flux swing $\Delta\Phi_p$ and the net energy consumed ΔU_p can be determined by integration of Eq. (24):

$$\begin{aligned} \Delta\Phi_p &= \int V_p\, dt = \int_0^{I_{\text{pf}}} \left(L + \pi a^2 A \frac{d\langle B_t \rangle}{dI_p} \right) dI_p, \\ \Delta U_p &= \int V_p I_p\, dt = \int_0^{I_{\text{pf}}} \left(L + \pi a^2 A \frac{d\langle B_t \rangle}{dI_p} \right) I_p\, dI_p. \end{aligned} \tag{33}$$

For the toroidal-field circuit, the flux swing $\Delta\Phi_t$ and the net energy consumed ΔU_t can be determined similarly:

$$\begin{aligned} \Delta\Phi_t &= \int V_t\, dt = \pi a^2 \int_0^{I_{\text{pf}}} \frac{d\langle B_t \rangle}{dI_p}\, dI_p, \\ \Delta U_t &= \int V_t I_t\, dt = \frac{2\pi^2 a^2 R_0}{\mu_0} \int_0^{I_{\text{pf}}} F \langle B_t \rangle \frac{d\langle B_t \rangle}{dI_p}\, dI_p. \end{aligned} \tag{34}$$

To these values must be added the flux and energy requirements to achieve the initial toroidal field $\langle B_{ti} \rangle$, which in general is not zero when the plasma current begins to increase:

$$\begin{aligned} \Delta\Phi_{ti} &= \pi a^2 \langle B_{ti} \rangle, \\ \Delta U_t &= \pi^2 a^2 R_0 \langle B_{ti} \rangle^2 / \mu_0. \end{aligned} \tag{35}$$

The integrands in Eqs. (33) and (34) are not unique functions of I_p but rather involve the variation of $\langle B_t \rangle$ with I_p over which one has some experimental control. In the sections to follow, five special cases will be considered. The first three cases will involve a current increase at a relatively low value of θ, and thus Eqs. (26) and (28) can be expanded to give the approximate values

$$L \simeq (\tfrac{3}{8} + \theta^2/2)\mu_0 R_0, \qquad A \simeq (1 - \theta^2)\theta R_0/2a. \tag{36}$$

With $F(\theta)$ from Eq. (17), these expressions simplify the integrations.

A. Ramped mode

Consider first the case in which $\langle B_t \rangle$ is a linear function of I_p, corresponding to a ramp-up at a constant value of θ. Equations (33) and (34) give

$$\begin{aligned} \Delta\Phi_p &= (\tfrac{5}{8} + \theta_f^2/4)\mu_0 R_0 I_{\rm pf}, \\ \Delta U_p &= (\tfrac{5}{16} + \theta_f^2/8)\mu_0 R_0 I_{\rm pf}^2, \\ \Delta\Phi_t &= \mu_0 a I_{\rm pf}/2\theta_f, \\ \Delta U_t &= (1/4\theta_f^2 - \tfrac{1}{8})\mu_0 R_0 I_{\rm pf}^2. \end{aligned} \tag{37}$$

Note that ΔU_t is positive for $\theta_f^2 < 2$ and negative for $\theta_f^2 > 2$ and that $\theta^2 = 2$ is the value for which $F = 0$. This means that the external toroidal-field circuit must supply energy for a nonreversed ramp-up and must sink energy for a reversed ramp-up. A ramp-up at $F = 0$ involves no energy flow and could in principle be accomplished with the toroidal-field winding open circuited as with a spheromak. A ramp-up at negative F requires an external inductance in the toroidal-field circuit with a value given by

$$L_{\rm ext} = -\frac{V_t}{dI_t/dt} = -\frac{\mu_0 a^2}{2R_0 F} \tag{38}$$

or in terms of the internal toroidal inductance $L_{\rm int}$ in the absence of plasma, $L_{\rm ext} = -L_{\rm int}/F$. Alternately, note that

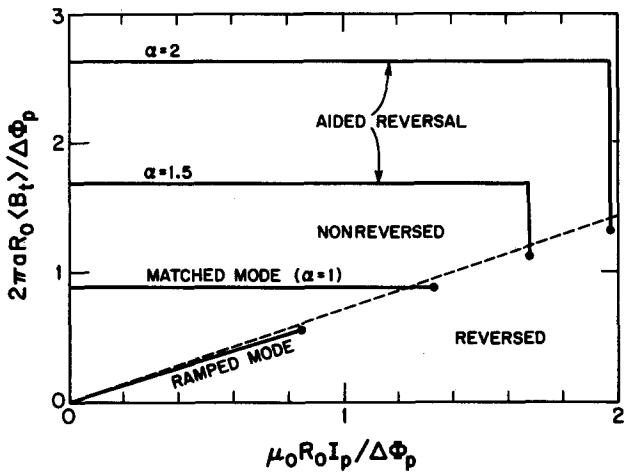

FIG. 9. Summary of RFP start-up modes showing trajectories through $\langle B_t \rangle$-I_p space, all of which end at the same value of $\theta_f = 1.5$. Note that for a fixed value of poloidal flux swing $\Delta\phi_p$, one can reach successively higher final plasma current values with matched mode and with aided reversal. Within limits, the higher the initial toroidal field, the higher plasma current that can be reached. Plasma resistance and external circuit losses have been neglected.

$I_t/I_p = R_0 F/a\theta$ is a constant for ramped mode, and thus a single power supply could drive the two circuits in series through appropriate transformers to produce the desired current ratio. In practice, it may be different to start up a RFP without an initial toroidal field, but the result represents an ideal limit.

Figure 9 shows the trajectory through $\langle B_t \rangle$-I_p space for this ramped mode case for $\theta_f = 1.5$. In the figure, I_p is normalized to $\Delta\Phi_p/\mu_0 R_0$ and $\langle B_t \rangle$ is normalized to $\Delta\Phi_p/2\pi a R_0$ so as to make the plot device independent with axes whose ratio is θ.

B. Matched mode

Consider now the case in which the toroidal flux is held constant as the plasma current increases. Constant $\langle B_t \rangle$ implies $V_t = 0$ (toroidal winding perfectly crowbarred) and all the flux swing and energy flow in the toroidal-field circuit occur before the plasma current begins to increase. Equations (33) and (35) give

$$\begin{aligned} \Delta\Phi_p &= (\tfrac{3}{8} + \theta_f^2/6)\mu_0 R_0 I_{\rm pf}, \\ \Delta U_p &= (\tfrac{3}{16} + \theta_f^2/8)\mu_0 R_0 I_{\rm pf}^2, \\ \Delta\Phi_t &= \mu_0 a I_{\rm pf}/2\theta_f, \\ \Delta U_t &= \mu_0 R_0 I_{\rm pf}^2/4\theta_f^2. \end{aligned} \tag{39}$$

As compared with ramped mode at the same $I_{\rm pf}$ and θ_f, this matched mode requires less poloidal flux and poloidal-field source energy but more toroidal-field source energy. Thus for a given poloidal flux swing, a higher plasma current can be reached as shown in Fig. 9. The toroidal flux swing and the total energy,

$$\Delta U = (1/4\theta_f^2 + \tfrac{3}{16} + \theta_f^2/8)\mu_0 R_0 I_{\rm pf}^2, \tag{40}$$

are the same for the two cases since they depend only on the final state and not on how it was reached. Equation (40) overpredicts the energy requirement by 8% at $\theta_f = 1.5$ and 24% at $\theta_f = 2.0$ as compared with Eq. (22) because of the approximations used. Note that for a fixed plasma current, the magnetic energy has a minimum of $0.541\mu_0 R_0 I_p^2$ at $\theta^4 = 2$, corresponding to $F = 0.302$.

C. Aided reversal

Consider now the more general case in which the average toroidal field is held fixed at $\alpha\langle B_{\rm tf} \rangle$ until the plasma current reaches its final value and then is readjusted to $\langle B_{\rm tf} \rangle$ while the plasma current is held constant. Matched mode is thus a special case of this aided reversal case in which $\alpha = 1$. For $\alpha \gg 1$, the maximum toroidal flux swing and energy consumption occur before the plasma current begins to increase. For α less than about $\exp(\theta_f^2/2)$, the poloidal flux swing and energy consumption are maximum when the final state is reached. For α within this range, Eqs. (33) and (35) give

$$\begin{aligned} \Delta\Phi_p &= (\tfrac{3}{8} + \theta_f^2/8 + \theta_f^2/24\alpha^2 - \ln\alpha/4)\mu_0 R_0 I_{\rm pf}, \\ \Delta U_p &= (\tfrac{3}{16} + \theta_f^2/8 - \ln\alpha/4)\mu_0 R_0 I_{\rm pf}^2, \\ \Delta\Phi_t &= \alpha\mu_0 a I_{\rm pf}/2\theta_f, \\ \Delta U_t &= \alpha^2 \mu_0 R_0 I_{\rm pf}^2/4\theta_f^2. \end{aligned} \tag{41}$$

Aided reversal further reduces the flux swing and energy requirements of the poloidal-field source as Fig. 9 shows for $\alpha = 1.5$ and $\alpha = 2$. The reduction is at the expense of a considerably increased toroidal flux swing and energy consumption, however.

A number of other start-up cases have been investigated numerically, but the results are unremarkable. Equation (41) predicts zero net poloidal flux swing and energy consumption for sufficiently large α, but this is because the poloidal flux and energy supplied during the rising I_p is removed when $\langle B_t \rangle$ is reduced to its final value.

D. Theta pinch mode

It is interesting to ask whether there is a trajectory through $\langle B_t \rangle$-I_p space for which the voltage V_p is always zero. Such a case would correspond to putting all the flux and energy in through the toroidal-field circuit as in a theta pinch. From Eq. (24) with V_p and R_p equal to zero using Eq. (2), we obtain

$$\frac{dI_p}{d\langle B_t \rangle} = -\frac{\pi a^2 A}{L}. \tag{42}$$

Since A and L depend on I_p and $\langle B_t \rangle$ in a complicated way, Eq. (42) is not easily integrated, but note that since A is zero at $\theta = 1$, I_p is maximum there. For small θ, the solution has $I_p \langle B_t \rangle^{2/3}$ constant. Equation (42) has been solved numerically using Eqs. (26) and (28), and the result is shown in Fig. 10. The result suggests that it is not possible to reach the RFP state in this way starting with zero plasma current. However, if one could produce a seed current in a toroidal device with a large initial toroidal magnetic field, the RFP state can apparently be reached by ramping the toroidal field down while the plasma current increases and then decreases slightly.

E. Oscillating field current drive

Consider now a case in which the toroidal-field and poloidal-field circuits are driven with voltages that are sinusoidal functions of time but with phases that differ by ϕ:

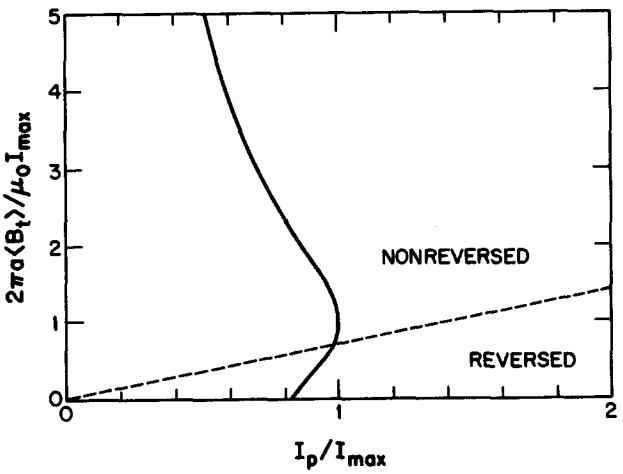

FIG. 10. Trajectory through normalized $\langle B_t \rangle$-I_p space for a case in which no poloidal-field driving voltage is used. The RFP state is reached by decreasing the average toroidal field from a large (infinite) initial value.

$$V_t = v_t \cos \omega t, \qquad V_p = v_p \cos(\omega t - \phi). \tag{43}$$

The frequency ω is arbitrary except that it is assumed sufficiently small that the plasma remains on the F-θ curve during an oscillation period. The field $\langle B_t \rangle$ averaged over any integral number of cycles of the oscillation is constant, and no net flux is supplied by either circuit. However, because of the nonlinearity of the equations, it is possible to rectify the alternating voltages and to compensate for resistive losses or even increase the current over time.[5,25–35] Such a technique is variously called oscillating field current drive, F-θ pumping, or helicity injection. We consider here the case of maintaining a constant current in the presence of plasma resistance.

Integrating Eq. (2) and Eq. (24) with $\omega \gg R_p/L$ gives

$$\langle B_t \rangle = \langle B_t \rangle_0 + v_t \sin \omega t / \pi a^2 \omega,$$
$$I_p = I_{p0} + v_p \sin(\omega t - \phi)/\omega L_0 - A v_t \sin \omega t / \omega L_0, \tag{44}$$

where the subscript 0 denotes the unperturbed ($v_p = v_t = 0$) values. Treating the oscillation as a small perturbation and using I_t from Eq. (4), one can average $I_p V_p$ and $I_t V_t$ over a cycle to obtain the power input to the plasma from each circuit:

$$P_p = -A v_p v_t \sin \phi / 2\omega L,$$
$$P_t = -R_0 v_p v_t \sin \phi \frac{dF/d\theta}{2a\omega L}. \tag{45}$$

Summing these powers and equating to the plasma Ohmic dissipation $I_p^2 R_p$, one can calculate the rectified voltage,

$$I_p R_p = -v_p v_t \sin \phi \frac{A + R_0 \, dF/d\theta \, /a}{2\omega L I_p}. \tag{46}$$

An equivalent result can be obtained by averaging Eq. (24) over a cycle of oscillation,

$$I_p R_p = v_p v_t \sin \phi \frac{\theta \, dA/d\theta + 2\theta^2 \, dL/d\theta \, /\mu_0 a}{2\omega L I_p}, \tag{47}$$

from which a nonobvious but possibly useful relation between L, A, and F can be deduced,

$$A + R_0 \frac{dF/d\theta}{a} = -\theta \frac{dA}{d\theta} - 2\theta^2 \frac{dL/d\theta}{\mu_0 a}. \tag{48}$$

Since the empirical fits for L, A, and F were not constructed to satisfy this constraint and since Eqs. (46) and (47) involve derivatives with respect to θ, the quantities cannot be accurately calculated from the fits but require an exact numerical evaluation from which Eq. (48) is verified.

For an appropriate choice of ϕ (optimum of $\pi/2$), it is possible to overcome the plasma resistive losses with such oscillating voltages and to maintain a constant average plasma current. The voltage $I_p R_p$ thus produced, normalized to $v_p v_t \sin \phi / \mu_0 a \omega I_p$, is plotted in Fig. 11 as a function of θ along with an empirical fit good to within 5% for $\theta < 2$,

$$I_p R_p \approx 9 v_p v_t \sin \phi \, \theta^2/(5 + 10\theta^2)\mu_0 a \omega I_p. \tag{49}$$

The plot illustrates the difficulty of using the technique for a tokamak ($\theta \ll 1$), although the low resistance of a tokamak discharge helps somewhat.

Note from Eq. (45) with $\sin \phi > 0$ that the toroidal-field

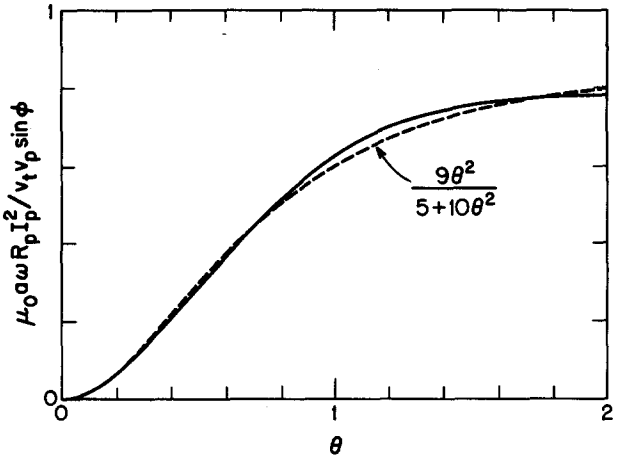

FIG. 11. Dimensionless coefficient that allows calculation of the value of I_pR_p that can be sustained in steady state by oscillating field current drive with voltages v_p and v_t at frequency ω with phase difference ϕ.

circuit always has to supply power since $dF/d\theta$ is negative, but that the poloidal-field circuit supplies power for $\theta > 1$ (where $A < 0$) and sinks power for $\theta < 1$. Thus for application to a tokamak, one needs an active circuit only for the toroidal field, and the poloidal-field circuit can be connected to a passive element. For $\phi = \pi/2$, such an element consists of an inductor, capacitor, and resistor all connected in parallel with values given by

$$\begin{aligned} &L_{\text{ext}} \gg L, \\ &C_{\text{ext}} = 1/\omega^2 L, \\ &R_{\text{ext}} = \omega L v_p / A v_t. \end{aligned} \tag{50}$$

The inductor provides a dc path for the unperturbed plasma current, the capacitor sets the phase, and the resistor allows one to adjust the ratio of v_p/v_t. The tokamak case is even less inherently efficient than the RFP case because some of the power supplied by the toroidal-field circuit is wasted in R_{ext}. The efficiency, defined by $I_p^2 R_p/P_t$, is predicted to be about 50% in the limit of small θ.

V. APPLICATION TO MST

In this section, the previous results will be applied to the Madison symmetric torus.[6] MST is a circular cross section RFP with $R_0 = 1.5$ m and $a = 0.52$ m. The poloidal flux is coupled by an iron core with a 2.0 Wb maximum flux swing. The toroidal magnetic field is produced by currents in the 5 cm thick, aluminum vacuum vessel wall which has a single toroidal and poloidal gap to allow the respective fields to enter. Protrusions of diagnostics and gap protectors are limited to a 1 cm thick region adjacent to the wall. There is no resistive liner.

A. Ultimate performance

The ultimate performance of the device occurs when the plasma resistance contributes negligibly to the flux and energy consumption. The capacitor banks and toroidal-field transformer can be upgraded arbitrarily, but the poloidal flux swing is limited to 2.0 Wb by the available space through the center of the toroid. Initial operation will approximate the ramped mode condition, but matched mode and aided reversal are future possibilities. From Eqs. (37), (39), and (41), Table I summarizes the ultimate performance for various start-up modes in which the pinch parameter reaches $\theta_f = 1.5$ at the peak of the plasma current.

TABLE I. Summary of ultimate performance parameters for various start-up modes of MST for $\Delta\phi_p = 2.0$ Wb and $\theta_f = 1.5$.

	Ramp	mm	Aided reversal $\alpha = 1.5$	Aided reversal $\alpha = 2.0$	
I_{pf}	0.89	1.41	1.78	2.10	MA
$\langle B_{ti}\rangle$	0.00	3.63	6.84	10.75	kG
$\langle B_{tf}\rangle$	2.29	3.63	4.56	5.37	kG
U_p	0.89	1.77	2.19	2.44	MJ
U_t	−0.02	0.42	1.49	3.68	MJ
$\Delta\phi_t$	0.20	0.31	0.87	1.83	Wb

B. Waveforms

The time-dependent waveforms for MST were determined by a numerical simulation of the plasma connected to a simplified representation of the external circuitry. More complicated and realistic simulations of the actual circuit have been performed, but the essence of the model is contained in Fig. 12. For convenience and in order to illustrate the numerical method, the basic equations are collected below:

$$\begin{aligned} &\text{Initialize } I_p,\ \langle B_t\rangle,\ V_p, \\ &\theta = \mu_0 I_p/2\pi a\langle B_t\rangle, \\ &L = 9\mu_0 R_0(2+3\theta^2)/8(6+\theta^2), \\ &A = 4R_0\theta(1-\theta^2)/a(8+3\theta^3), \\ &R_p = f(I_p), \\ &F = 1-\theta^2/2, \\ &I_t = 2\pi R_0\langle B_t\rangle F/\mu_0, \\ &V_t = -L_{\text{ext}}\frac{dI_t}{dt}, \\ &\frac{d\langle B_t\rangle}{dt} = \pi a^2 V_t, \\ &\frac{dV_p}{dt} = -\frac{I_p}{C}, \\ &\frac{dI_p}{dt} = \frac{V_p - AV_t - I_pR_p}{L}. \end{aligned} \tag{51}$$

The initial values were taken as $I_p = 0$, $\langle B_t\rangle = 875$ G (to allow for electron cyclotron resonance preionization at 2.45 GHz), and $V_p = 125$ V (5 kV/40 turns). The param-

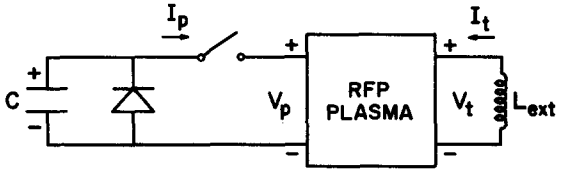

FIG. 12. Simplified electrical circuit for numerical simulation of the time-dependent response of a RFP plasma.

eters chosen were $C = 168$ F (to give $\Delta\Phi_p = 2.0$ Wb) and $L_{ext} = 0.265\ \mu$H (to give $\theta_f = 1.5$). Here R_p was assumed to be given by Eq. (30) with η from Eq. (31) with $Z_{eff} = 5$ and $T_e = 10^{-3} I_p$ (OHTE scaling[36]). To avoid a singularity in R_p at $t = 0$, a lower bound for T_e was taken to be 0.1 eV, a value that surely can be achieved with low-power electron cyclotron resonance preionization.

One computational difficulty is the necessity of evaluating a derivative in order to calculate V_t from dI_t/dt. This process leads to numerical instability unless L_{ext} is very small or $I_t(t)$ is suitably smoothed. Such smoothing can be accomplished by adding to the circuit a resistor R_{ext} in parallel with L_{ext} chosen such that $V_t/I_t \ll R_{ext} \ll L_{ext}/\Delta t$, where Δt is the step size of the iteration. The value is large enough so as to draw negligible current but small enough so that the time constant of the external circuit exceeds the iteration time step. When simulating a device with a resistive liner, such a resistance naturally exists, and the problem does not occur.

The waveforms predicted by the simulation are shown in Fig. 13. The case is intermediate between the ramped mode and matched mode cases of Sec. IV. The plasma current I_p reaches a maximum of 1.16 MA at about 25 msec, at which time $R_p I_p$ is 4.32 V. Beyond about 50 msec, field errors are expected to arise, raising the resistivity and eventually terminating the discharge. The total energy delivered by the poloidal-field and toroidal-field sources is 1.38 MJ, 93% of which is stored inductively at the time of peak current. The inductive energy consumed by the plasma agrees within 7% with the stored magnetic energy calculated from

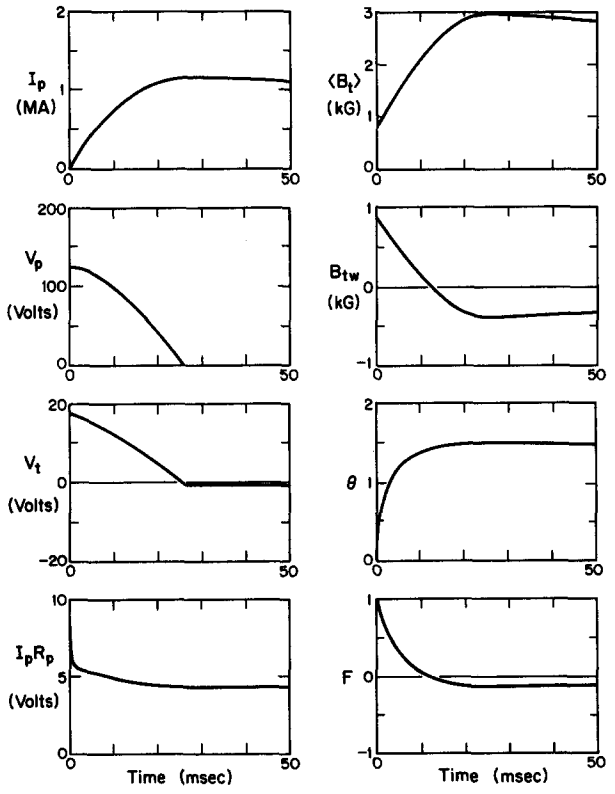

FIG. 13. Results of numerical simulation of MST waveforms for maximum flux swing ($\Delta\phi_p = 2.0$ Wb) and an optimistically low plasma resistance.

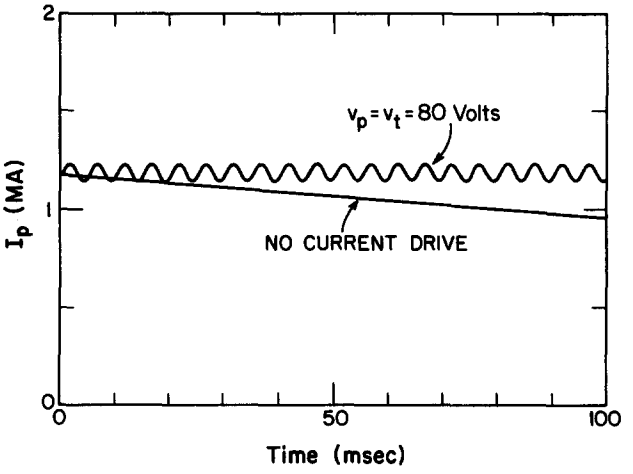

FIG. 14. Numerical simulation of oscillating field current drive applied to MST to maintain a constant average plasma current for an optimistically low plasma resistance.

Eq. (22) providing a check of many aspects of the calculation. This case represents a reasonable upper bound of the initial performance that can be expected from MST.

C. Oscillating field current drive

If the loop voltage in MST can be reduced to the order of 4 V as suggested above, the device might be useful for testing oscillating field current drive. To simulate such a case, the parameters of Sec. V B at the peak of the plasma current were taken as initial values, and the toroidal-field and poloidal-field voltages were taken according to Eq. (43) with $v_t = v_p = 80$ V, $\omega/2\pi = 200$ Hz, and $\phi = \pi/2$ as required to hold the average plasma current constant.

The plasma current for the following 100 msec is shown in Fig. 14 along with the corresponding value for $v_t = v_p = 0$. The onset of field errors might preclude such long pulses, however. The variation in F is such that the plasma barely goes out of reversal ($F = 0$) at the peak of each cycle, although this could have been prevented by operating at slightly larger average θ. In the simulation, R_p is allowed to vary with θ according to Eq. (30), but no account is taken of any resistance enhancement when reversal is lost. If $I_p R_p$ is larger than assumed, more oscillating voltage is required, and it is difficult to maintain a reversed field state throughout the oscillation. The 80 V value is in good agreement with the 75 V predicted by Eq. (46). The average power required to maintain the plasma is 5.32 MW, 3.90 MW of which comes from the toroidal-field source and 1.42 MW of which comes from the poloidal-field source in rough agreement with Eq. (45).

The poloidal-field circuit is primarily resistive, but the toroidal-field circuit has an inductive reactance that is roughly four times its resistance. This raises the possibility of driving the two circuits in series from the same source and letting the plasma provide the phase shift. Provision would have to be made for the fact that the dc currents in the two circuits are different, and in fact, opposite in sign for $F < 0$. This could easily be accomplished by inductors in parallel with each circuit.

ACKNOWLEDGMENTS

The author is grateful to Professor D. W. Kerst and Professor S. C. Prager for a critical reading of the manuscript.

This work was supported by the U.S. Department of Energy grant No. DE-FG02-85ER53198.

[1]H. A. B. Bodin and A. A. Newton, Nucl. Fusion **20**, 1255 (1980).
[2]D. A. Baker and W. E. Quinn, in *Fusion*, edited by E. Teller (Academic, New York, 1981), Vol. I, Part A, Chap. 7.
[3]J. W. Johnson, Plasma Phys. **23**, 187 (1981).
[4]K. F. Schoenberg, R. F. Gribble, and J. A. Phillips, Nucl. Fusion **22**, 1433 (1982).
[5]K. F. Schoenberg, R. F. Gribble, and D. A. Baker, J. Appl. Phys. **56**, 2519 (1984).
[6]A. F. Almagri, S. Assadi, J. Beckstead, G. Chartas, R. N. Dexter, D. J. Den Hartog, Y. L. Ho, D. W. Kerst, T. W. Lovell, S. C. Prager, J. S. Sarff, W. Shen, C. Spragins, and J. C. Sprott, Bull. Am. Phys. Soc. **23**, 1830 (1987).
[7]J. B. Taylor, Phys. Rev. Lett. **33**, 1139 (1974).
[8]R. J. Bickerton, Proc. Phys. Soc. **72**, 618 (1958).
[9]K. J. Whiteman, Plasma Phys. **7**, 293 (1965).
[10]M. G. Rusbridge, Plasma Phys. **19**, 499 (1977).
[11]A. Bhattacharjee and R. L. Dewar, Phys. Fluids **25**, 887 (1982).
[12]V. Antoni and S. Ortolani, Phys. Fluids **30**, 1489 (1987).
[13]K. K. Jain, Phys. Lett. A **126**, 269 (1988).
[14]V. Antoni and S. Ortolani, Plasma Phys. **25**, 799 (1983).
[15]R. J. La Haye, T. N. Carlstrom, R. R. Goforth, G. L. Jackson, M. J. Schaffer, T. Tamano, and P. L. Taylor, Phys. Fluids **27**, 2576 (1984).
[16]J. S. Sarff, J. C. Sprott, and L. Turner, Phys. Fluids **30**, 2155 (1987).
[17]D. J. Lees and M. G. Rusbridge, in *Proceedings of the 4th International Conference on Ionization Phenomena in Gases 2* (North-Holland, Amsterdam, 1960), p. 954.
[18]W. M. Burton, E. P. Butt, H. C. Cole, A. Gibson, D. W. Mason, R. S. Pease, K. Whiteman, and R. Wilson, Nucl. Fusion: 1962 Suppl. Pt. 3, 903 (1962).
[19]H. A. B. Bodin and D. E. Evans, Nucl. Fusion **25**, 1305 (1985).
[20]A. Buffa, S. Costa, R. Gianella, G. Malesani, G. F. Nalesso, and S. Ortolani, in *Plasma Physics and Controlled Nuclear Fusion Research* (IAEA, Vienna, 1977), Vol I, p. 447.
[21]T. Shimada, Y. Hirano, Y. Maejima, and K. Ogawa, in *Plasma Physics and Controlled Nuclear Fusion Research* (IAEA, Vienna, 1977), Vol I, p. 463.
[22]H. K. Moffatt, *Magnetic Field Generation in Electrically Conducting Fluids* (Cambridge U.P., Cambridge, 1978).
[23]L. Turner and J. P. Christiansen, Phys. Fluids **24**, 893 (1981).
[24]L. Spitzer and R. Harm, Phys. Rev. **89**, 977 (1953).
[25]M. K. Bevir and J. W. Gray, in *Proceedings of the Reversed Field Pinch Theory Workshop* (Los Alamos National Laboratory, Los Alamos, NM, 1981), p. 1976.
[26]C. G. Bathke, M. J. Embrechts, R. L. Hagenson, R. A. Krakowski, and R. L. Miller, in *Proceedings of the 10th Symposium on Fusion Engineering*, Philadelphia (IEEE, New York, 1983), p. 853.
[27]K. F. Schoenberg, C. J. Buchenauer, R. S. Massey, J. G. Melton, R. W. Moses, R. A. Nebel, and J. A. Phillips, Phys. Fluids **27**, 548 (1984).
[28]T. H. Jensen and M. S. Chu, Phys. Fluids **12**, 2881 (1984).
[29]P. M. Bellan, Phys. Fluids **27**, 2191 (1984).
[30]M. K. Bevir, C. G. Gimlett, and G. Miller, Phys. Fluids **28**, 1826 (1985).
[31]P. M. Bellan, Phys. Rev. Lett. **54**, 1381 (1985).
[32]P. M. Bellan, Phys. Rev. Lett. **57**, 2383 (1986).
[33]J. M. Finn, Phys. Fluids **29**, 2630 (1986).
[34]H. R. Strauss and D. S. Harned, Phys. Fluids **30**, 164 (1987).
[35]P. M. Bellan, Phys. Fluids **31**, 215 (1988).
[36]T. Tamano, W. D. Bard, T. N. Carlstrom, C. Chu, B. Curwen, R. K. Fisher, D. W. Graumann, R. R. Goforth, G. L. Jackson, R. J. La Haye, T. Ohkawa, M. J. Schaffer, M. T. Saito, P. L. Taylor, T. S. Taylor, D. F. Register, and S. E. Walker, in *Plasma Physics and Controlled Nuclear Fusion Research* (IAEA, Vienna, 1985), Vol. II, p. 431.